

ОБЪЕДИНЕННЫЙ
ИНСТИТУТ
ЯДЕРНЫХ
ИССЛЕДОВАНИЙ
ДУБНА

E15-94-64

A. V. Yeremin, A. N. Andreyev, D. D. Bogdanov,
G. M. Ter-Akopian, V. I. Chepigin, V. A. Gorshkov,
A. P. Kabachenko, O. N. Malyshev, A. G. Popeko,
R. N. Sagaidak, S. Sharo*, E. N. Voronkov,
A. V. Taranenko, A. Yu. Lavrentjev

THE KINEMATIC SEPARATOR VASSILISSA –
PERFORMANCE AND EXPERIMENTAL RESULTS¹

Submitted to «Nuclear Instruments and Methods in Physics Research,
Section A»

*Comenius University, Bratislava, Slovakia

¹This work was supported in part by the Russian Foundation
of Fundamental Research (contract N 93-02-3750)

1994

Кинематический сепаратор ВАСИЛИСА – современное состояние и результаты экспериментов

Кинематический сепаратор ВАСИЛИСА в течение последних пяти лет использовался для исследования нейтрон-дефицитных ядер – испарительных продуктов реакций слияния с тяжелыми ионами. В процессе этой работы была проведена оптимизация ионно-оптической и других систем сепаратора, включая усовершенствование детектирующей системы в фокальной плоскости. В результате получены величины эффективности сепарации ядер – испарительных продуктов от 3 до 30% для реакций с налетающими ионами от ^{16}O до ^{40}Ar . Факторы подавления фоновых продуктов составили $>10^{19}$ для ионов пучка с полной энергией и $>10^4$ для продуктов реакций многонуклонных передач.

Кратко представлены результаты выполненных экспериментов.

Работа выполнена в Лаборатории ядерных реакций ОИЯИ.

Препринт Объединенного института ядерных исследований. Дубна, 1994

The Kinematic Separator VASSILISSA – Performance and Experimental Results

For the last five years the kinematic separator VASSILISSA [1,2] has been used for investigations of neutron deficient evaporation residues (ER) produced in heavy ion fusion reactions. In the course of this work optimization of the ion-optical and other systems of the separator including improvements of the focal plane detector system have been made. As a result, the separation efficiency values ranging from 3 to 30% were achieved for ER's produced in the reactions with heavy ions ranging from ^{16}O to ^{40}Ar . The suppression factors $>10^{19}$ for the full energy beam particles and $>10^4$ for multinucleon transfer reaction products were achieved.

The results of the performed experiments are briefly presented.

The investigation has been performed at the Laboratory of Nuclear Reactions, JINR.

1 Introduction

In the transfermium region of nuclei subnanobarn cross sections of heavy ion fusion evaporation reactions and, as a result, vanishing low yields of the nuclides being of interest make the study difficult. Higher production cross sections are obtained for the isotopes of the elements having $Z \leq 94$. However in this region the study of extremely neutron-deficient nuclides is complicated by presence of the background of different neighboring nuclides. Nevertheless, despite these difficulties, heavy ion fusion reactions were studied in these region of compound nuclei during the last few years making use of kinematic separators. Such separators were build in many laboratories (see for example [3] and references therein).

Apart from the fact that the real progress in the development of this technique is evident, further work is needed to increase the separation efficiency, especially for the case of the asymmetric fusion reactions, and the suppression factors of the background particles.

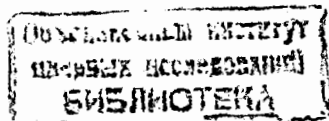
Our experiments were carried out with the kinematic separator VASILISSA [1] designed for the observation of heavy evaporation residues (ER's) produced as a result of fusion reactions induced by relatively light ($A \leq 40$) bombarding ions. The fusion reactions leading to the formation of neutron-deficient nuclides with $Z \geq 83$ were the subject of our study [4] including the reactions being of interest for the synthesis of the heavy nuclei with $Z \geq 100$ [5, 6, 7].

2 Experimental set-up

The kinematic separator VASSILISSA was installed in 1987 on the beam of the U-400 heavy ion cyclotron of the FLNR JINR and since then was used in experiments.

The projectile beams used in our experiments were as follows: $^{16,18}\text{O}$, $^{20,22}\text{Ne}$, $^{24,26}\text{Mg}$, ^{27}Al , ^{31}P , ^{40}Ar and ^{40}Ca . The U-400 cyclotron produces the beams in the pulsed mode at the modulation frequency of $f=150$ Hz and the duty factor of $\approx 25\%$. The beam intensity on the separator target (10 mm in the diameter) was typically $(0.3 - 10.0) \times 10^{12} \text{s}^{-1}$.

The beam energy was controlled by measuring the energy of the ions scattered at 30° in a thin ($200 \mu\text{g}/\text{cm}^2$) gold foil. Foils of Al and Ti were used as degraders to vary smoothly the beam energy. The typical energy



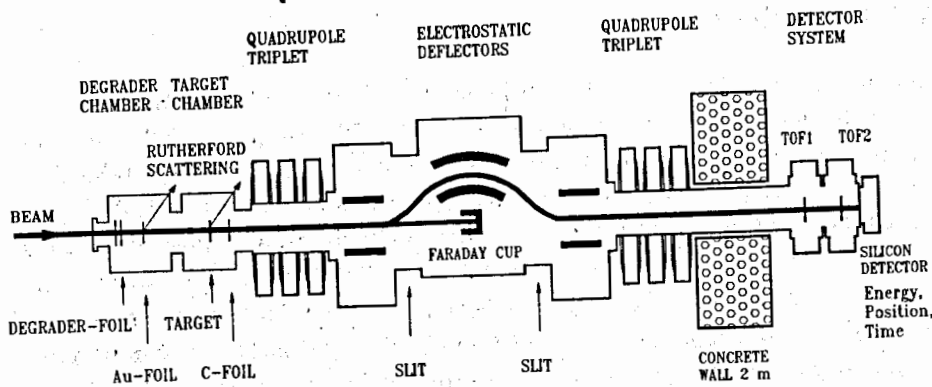


Fig. 1. Schematic view of the kinematic separator VASSILISSA.

spread of bombarding ions was $\approx (1 - 1.5)\%$.

2.1 Description of VASSILISSA

Schematic view of the experimental set-up is presented in Fig. 1.

The principal component of the VASSILISSA facility is a system consisting of three electrostatic dipoles, which accomplish the spatial separation of the trajectories of recoil nuclei, multinucleon transfer reaction products and beam particles by virtue of differences in their energy and ionic charges.

Complete fusion reaction products with the mass $A_{cn} = A_p + A_t$ leave the target in the beam direction and have the energy:

$$E_{cn} = \frac{A_p}{A_p + A_t} \cdot E_p,$$

where E_p is the projectile energy, A_p and A_t are the mass numbers of the projectile and target nuclei. The deflection angle of an ion of the energy E and charge state q in an electric field is proportional to the value q/E and, so,

$$\frac{\alpha_{cn}}{\alpha_p} \approx \frac{(A_p + A_t)}{A_p} \cdot \frac{q_{cn}}{q_p}, \quad (1)$$

where α_{cn} and α_p are the deflection angles for the recoil nucleus and projectile, respectively.

Recoil nuclei are deflected in the first dipole by 8° to enter the second dipole aperture whereas the full energy projectiles pass through the first

Table 1. Typical operating parameters of VASSILISSA.

Maximum particle current on target	$1 \times 10^{13} \text{s}^{-1}$
Target diameter	10 mm
Target thickness	100–500 $\mu\text{g}/\text{cm}^2$
Accepted angle	$140 \times 140 \text{ mrad}^2$
Solid angle	15 msr
Accepted energy range	$\pm 15\%$
Efficiency	3–30%
Overall background rejection	$10^{11} - 10^{13}$
Quadrupole aperture (radius)	100 mm
Maximum field gradient	10 T/m
Maximum value of electric field strength	20 kV/cm

dipole almost unperturbed and then are stopped in the Faraday cup. Further separation of recoil nuclei from scattered projectiles and other background particles takes place in the second and third dipoles. Electric rigidity is the same for three dipoles. The design goal for its maximum value was 2.5 MV.

The focusing system of VASSILISSA consists of two triplets of broad aperture magnetic quadrupoles. The first triplet located just behind the target focuses the ER's knocked out of the target and shapes their flux into a quasiparallel beam. The second triplet follows the electric dipoles and serves for collecting the flux of the ER's onto the focal plane detectors.

The thicknesses of our separator targets are typically $(150 - 500) \mu\text{g}/\text{cm}^2$. In the case of the high beam intensity ($10^{12} - 10^{13} \text{s}^{-1}$), the target mounted on a rotating wheel is used. The rotation of the target wheel is synchronized with the cyclotron beam pulses. Recoil nuclei emerging from the target are accepted by the separator within a solid angle of 15 msr ($\approx \pm 4^\circ$ in the vertical and horizontal directions). VASSILISSA tolerates the energy and charge deviations of up to $\pm 15\%$. The distance from the target to the focal plane is about 12 m. Typical operating parameters of VASSILISSA are disposed in Table 1.

A care was taken in this work to improve the accuracy of the predictions for the energy, angular and charge distributions of the recoil nuclei emerging from the separator target. The precise knowledge of these distributions is essential for obtaining the maximum transmission of ER's

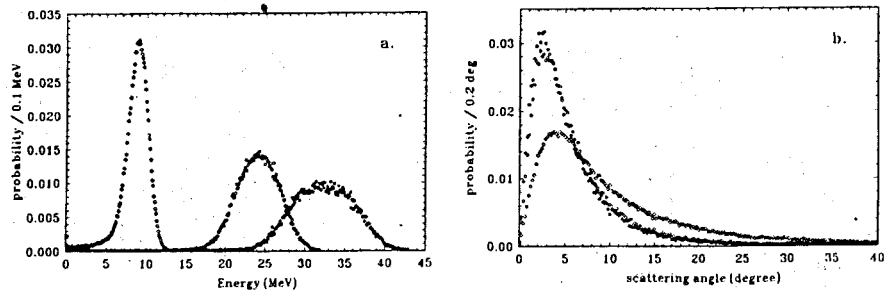
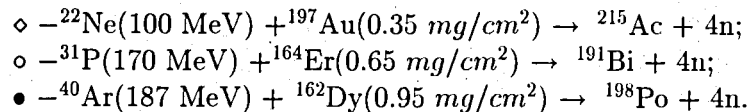


Fig. 2. Calculated energy (a) and angular (b) distributions for ER's from reactions:



and suppression of the background especially when the production cross sections of the investigated ER's are below few nanobarns. This is also important for the accurate evaluations of the separator efficiency when precise measurements are carried out for the reaction cross sections.

The evaporation residues from asymmetric heavy ion fusion reactions cover a broad angular and energy ranges, which come from the deexcitation of the compound nuclei by the evaporation of neutrons and/or protons and α -particles. The widths of these distributions are enlarged further through scattering and energy losses in the target.

We made some refinement of the calculation methods for energy and angular distributions of ions passing through the solid media [8, 9]. Fig. 2 shows some ER's energy and angular distributions calculated with the Monte-Carlo computer code [9] for the targets with the thicknesses, which are optimized for the maximum ER yield.

Evaporation residues leave the target in excited states, and a cascade of Auger electrons increases their mean charge and makes the charge distribution extremely broad [10]. To reset the charge distribution to the equilibrium, a thin ($20\text{--}30 \mu\text{g/cm}^2$) carbon foil is placed eight centimeters downstream of the target. The optimal foil thickness for the charge equilibration can be chosen according to [11]. At the residual gas pressure of about 10^{-6} Torr in the vacuum volume of the separator nearly all the ER's reach the focal plane detector without charge changing collisions. Therefore the precise knowledge of the mean equilibrium charge \bar{q} and

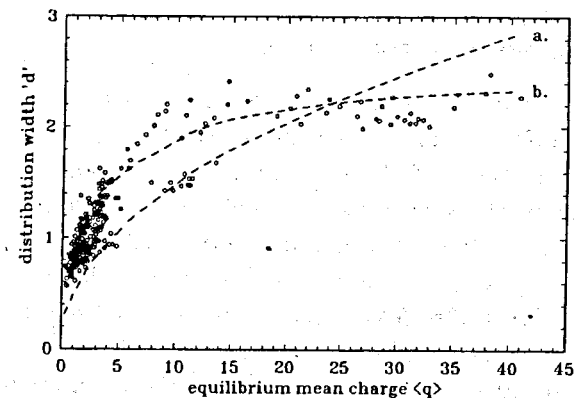


Fig. 3. Charge distribution widths of ions after passing of carbon foils as a function of the mean charge $\langle q \rangle$: ○ – experimental data; calculated data (a) – from [15], (b) – from [17].

charge distribution width d_q of ions after passing of the carbon foil is especially important for correct operation of the recoil separators.

Experimental data on \bar{q} and d_q reported before 1972 are summarized by Wittkower and Betz [12], those obtained between 1972 – 85 are compiled by Shima et al. [13], and more recent data published after 1985 are included in [14]. There are several approaches to estimate \bar{q} and d_q . The most popular are the formulae of Nikolaev and Dmitriev [15] and Shima, Ishihara and Mikumo [16].

The analysis [17] of the experimental data showed that the observed values of \bar{q} and d_q are poorly reproduced by the existing formulae for ions in the energy range of our interests ($0.01 \leq E \leq 0.1 \text{ MeV/amu}$). The deviation as large as 100% is quite possible. To improve the situation we developed the new semiempirical formulae giving the better agreement with the experimental data on the mean equilibrium charge and charge distribution width of the ions passing through carbon foils [17, 18].

The data on the charge distribution widths d_q are important for the calculations of the kinematic separator transport efficiency and background suppression. Fig. 3 shows the existing data on d_q and the data, calculated with the formulae [15] and [17]. Our formulae enable one to predict \bar{q} with an accuracy of $\approx 10\%$. Such an error in the assumed mean charge reduces the separator transmission by 15%.

2.2 Focal plane detector system

An array of silicon detectors and two (start and stop) time-of-flight detectors are installed in the separator focal plane. After passing the time-of-flight detectors [19], recoil nuclei are implanted into the silicon detectors. The working material of each of the two time-of-flight detectors is a thin ($30 \mu\text{g}/\text{cm}^2$) mylar foil covering a 80 mm diameter opening intended for the passage of the recoils. Secondary electrons emitted from the foil are accelerated to 5 keV in electric field and bend by a magnet to an array of microchannel plates [19]. The time resolution of about 0.5 ns was obtained for slow (full energy 10–20 MeV) recoil nuclei having mass numbers of about 200. The value of 99.95% was achieved with a single time-of-flight detector for the detection probability of such recoil nuclei.

The silicon detector array is assembled on the basis of separate position sensitive strips. Eight such strips having each the $(8 \times 64) \text{ mm}^2$ sensitive area compose the detector array with rectangular surface of $(67.5 \times 64) \text{ mm}^2$. The typical energy resolution is about 45 keV (FWHM) for 5.3 MeV α -particles. Position resolution is close to 0.5 mm in each strip.

The measurement of the time-of-flight and energy of the recoil nuclei yields their mass with an accuracy of about 10% thus allowing to separate ER's from target-like and beam-like particles using the two-dimensional TOF-Energy spectra. The anticoincidence condition for the signals from the time-of-flight and silicon detectors is used to distinguish between the pulses originating from the recoil nuclei and their α -decays, i.e. to obtain the "clean" α -spectra. To reduce the low-energy background of the scattered projectiles and to shift their energy distribution to lower energies (less than the region of 6–9 MeV characteristic of α -decay) the $200 \mu\text{g}/\text{cm}^2$ thick mylar degrader foil is inserted in front of the silicon detector array.

The heavy-ion fusion reaction products were unambiguously identified by the measured α -decay energies and life-times. In many cases identification was performed due to the observation of the time correlated α -decays of nuclides belonging to the known α -decay chains. This method was applied in each case when the identification of a previously unknown nuclides or α -decay lines was considered [20, 21].

3 Data acquisition system

The data acquisition system of VASSILISSA [22] allows us to store, event by event, the information about the energy, position, time-of-flight and arrival time of the recoil nuclei implanted into the focal plane detector, the position, detection time and energy of the recorded alpha decay and spontaneous fission events in the detectors. Some additional parameters are also recorded together with the codes of the events. The analog input signals are digitized and organized in events by CAMAC electronics. At present the total number of parameters in a typical experiment is 24.

A specially developed interface is used to transfer the data from CAMAC crates to the memory of the IBM PC AT/386 working under DOS 5.0 and PC NFS [23] with the use of DMA data transfer. The PC AT collects and filters events and sends them to the mass storage. The front-end PC is linked with thin ETHERNET cable to the main SUN IPX workstation which supervises the system and stores the data. The distance between PC AT and workstation is over 200 meters.

The data transfer rate from CAMAC to the hard disk is determined both by the transfer rates of the HDD and the ETHERNET link. In our experiments it reaches up to 300 KB/s.

A new version of the data analysis software is used for the on-line/off-line data analysis based on the CERN code PAW [24]. The PAW session organizes the graphical visualization of the data and supplies a powerful toolkit (based on the CERNLIB packages) for their analysis.

4 Separation efficiency

Let us define two terms:

- **separation efficiency:** the ratio of the number of the recoil nuclei recorded by the focal plane silicon detector array to the number of such nuclei produced in the target;
- **suppression factor:** the ratio of the number of the produced transfer reaction products or incident beam particles to those obtained by the focal plane detector.

In many cases, when the reaction cross-sections are in the nanobarn range and only few detected events per hour are expected the on-line

optimization of the separator setting is impossible. So, the calculations and calibrations of separation efficiency comprise a considerable part of the experimental work carried out with the separator. The accurate computer simulation is important for such case.

For calculations of the separation efficiency a Monte-Carlo computer code was developed [9]. The program takes into account and calculates the emittance of the projectile beam, reaction kinematics, momentum transfer from the evaporated particles – neutrons, protons or α 's to the ER, scattering and energy losses of ER's in the target and foils, the ionic charge distribution of ER's combined with the first order ion optics.

To calibrate the ion optical elements of the separator we used a ^{249}Cf α source placed in the target position and covered by a $10\ \mu\text{m}$ Al foil to reduce the α particle electric rigidity to the acceptable level. The α particles passing through the foil had the energy of 4.0 MeV and a relative energy spread of about 15%. The potentials of the electrostatic dipoles and field gradients of the magnetic quadrupoles coincided with the calculated values within 3% of accuracy. The α -particle spot obtained in the separator focal plane was 50 mm in diameter.

The separation efficiency of the facility was studied for ER's produced in asymmetric (HI,xn) and (HI, α xn) reactions which occurred between several projectile (O, Ne, Mg, P, Ar) and target (Dy, Er, Ta, W, Au, Pb) nuclei. The efficiency values ε_{xn} were derived by comparing the decay rates of the ER's implanted into the focal plane detector with the rates detected in a catcher foil placed just behind the target; α -spectra of known product nuclei were measured and their half-lives were determined. The measurements were performed for the targets of different thickness (w_t) ranging from 0.1 to 1 mg/cm².

Fig. 4 shows the experimentally measured efficiencies of ER's as a function of the target thickness together with the results of our calculations. One can see that the calculated and experimental values of the VASSILISSA efficiency coincide rather well. The fraction of the ER's passing through the separator entrance aperture range from 25% to 65% for the targets with the optimal thickness. The corresponding separation efficiencies are 5% for Ne, 10% for Al and 15% for Ar beams. The losses are caused by the energy and charge selection in VASSILISSA.

The investigation of the separation efficiency for (HI, α xn) reactions products – $\varepsilon_{\alpha xn}$ was performed for the $^{20,22}\text{Ne}$ and ^{24}Mg induced reac-

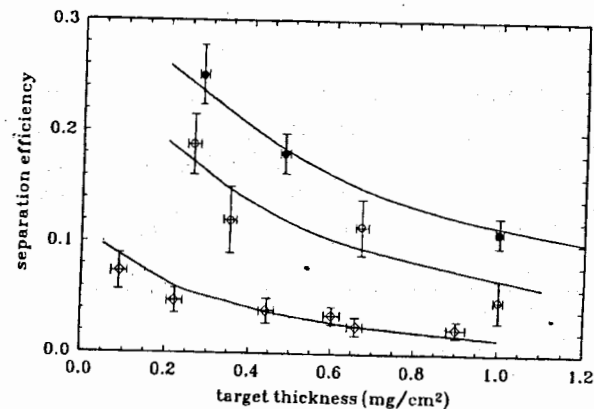
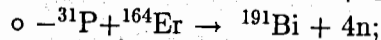
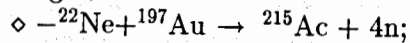


Fig. 4. Separation efficiency for different projectiles as a function of target thickness.



Calculated efficiency (lines) are shown for a comparison.

tions. For the reactions $^{20,22}\text{Ne} + ^{197}\text{Au}$ the ratio of $\varepsilon_{xn}/\varepsilon_{\alpha xn}$ was derived directly by comparison of the decay rates of the products emerging from xn and α xn reaction channels and being implanted into the focal plane detector and into the catcher foil. We could distinguish easily these product nuclei even in the catcher foil due to the significant differences in their α -decay energy. For the reaction $^{24}\text{Mg} + ^{197}\text{Au}$ the direct determination of ε_{xn} was impossible due to the short life time of protactinium isotopes with mass numbers $A \leq 218$. The separation efficiency for these products was derived from the data on ε_{xn} for the reactions $\text{Ne} + \text{W}$, $\text{Ne} + \text{Au}$ and $\text{Mg} + \text{Ta}$. Values of $\varepsilon_{\alpha xn}$ were determined by the technique of implantation into the separator focal plane Si detector and comparison of the obtained α -decay rate with that measured in the catcher foil placed just behind the separator target.

The results for the obtained ratios $\varepsilon_{xn}/\varepsilon_{\alpha xn}$ are presented in Table 2. The separation efficiency for the ER's produced via (HI, α xn) reactions – $\varepsilon_{\alpha xn}$ is lower than ε_{xn} due to much broader angular and energy distributions and also depends on the target thickness. With the increase of the target thickness the separation efficiency of recoil nuclei falls down, and the number of background products implanted into the detector –

Table 2. Measured values of the separation efficiency ratio $\varepsilon_{xn}/\varepsilon_{\alpha xn}$.

Reaction	w_t (mg/cm ²)	$\varepsilon_{xn}/\varepsilon_{\alpha xn}$	Reference
²⁰ Ne+ ¹⁹⁷ Au	0.4	6.1±0.6	[25]
²² Ne+ ¹⁹⁷ Au	0.6	8.0±2.0	[26]
²⁴ Mg+ ¹⁸¹ Ta / ¹⁹⁷ Au	0.2	25.0±5.0	[2]
	0.8	12.0±2.5	

increases.

For each experiment we carried out the measurements of the separation efficiency for properly chosen control reactions. For the whole set of the obtained data the relative errors in the measured cross sections are evaluated to be about 50% mainly due to the uncertainty of the separation efficiency. Other sources of the errors are, apart the statistics, the inhomogeneity of the target thickness and errors in the beam current measurements.

5 Suppression factors

An analysis using the time-of-flight and energy measurement showed that the scattered beam particles, elastically scattered target-like nuclei and multinucleon transfer reaction products having the same q/E ratio as the ER's to be investigated make the background obtained in the focal plane of the separator. For two target-projectile combinations (²²Ne+^{nat}W and ⁴⁰Ar+^{nat}Dy) leading to the same region of compound nuclei fig. 5 shows the time-of-flight - energy patterns, made by the particles arriving at the focal plane of the separator.

5.1 Suppression of beam-like projectiles

To limit the beam dimensions on the target we use the diaphragms with the diameter of 10-12 mm. Primary beam particles are scattered mainly from the diaphragm edges and target frames and typically have the energy from 1 to 20 MeV. This makes some problems with the registration of α -particles emitted by ER's implanted into the focal plane Si detector. The anticoincidence condition between the signals from the time-of-flight

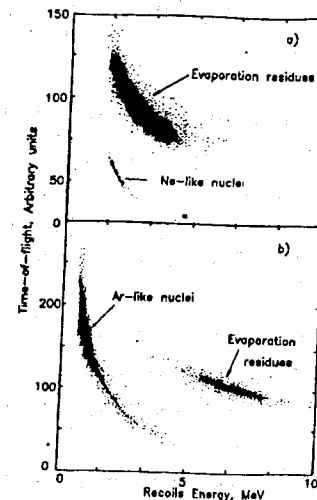


Fig. 5. Time-of-flight versus energy spectra measured at the VASSILISSA focal plane; (a) - for the reaction ²²Ne+^{nat}W, (b) - for the reaction ⁴⁰Ar+^{nat}Dy.

detectors and the energy signal from the Si detector was used to distinguish between the pulses originating from the background particles and ER's on one side and α -decay signals of the ER's, thus obtaining "clean" α -spectra. To reduce the background of the scattered projectiles and to shift their energy distribution to lower energies (less than α -energy region of the main interest - 6-9 MeV) the 200 $\mu\text{g}/\text{cm}^2$ mylar degrader was inserted in front of the silicon detector.

From eq. (1) follows the relative difference of the deflection angle of the beams of ER's and projectiles:

$$\frac{(\alpha_{cn} - \alpha_p)}{\alpha_{cn}} \approx \frac{A_t}{A_t + A_p} \quad (2)$$

for $q_{cn} \approx q_p$. It increases with decreasing mass of the projectile resulting in a higher background suppression. The largest relative difference in the deflection angles we had in the reactions of ions of ^{20,22}Ne on Au and Pb targets. In the separator focal plane we obtained only evaporation residues for these reactions.

Comparing with the beam intensity on the separator target, the flow of these beam ions passing through the time-of-flight detectors is sup-

pressed by the factor of 10^8 – 10^{10} depending on the projectile – target mass ratio. The count rate on the Si detectors is reduced by an additional factor of 10 – 30 because of absorption of the scattered ions in the time-of-flight detector foils and the foil installed before the Si detectors. Due to the measurement of the recoil time-of-flight and energy we additionally suppress this background by the factor of 100.

The overall background suppression ranges from 10^{13} – 10^{11} being dependent on the projectile to target mass ratio and also on the tuning of the U-400 beam.

To reduce the low energy background originating from the scattering of the beam on the edges of the diaphragms and target frame the doublet of magnetic quadrupole lenses was installed before the separator target position.

To reduce further this background we are planning to install an 8° degree dipole magnet between the second quadrupole triplet and focal plane. A computer simulation shows that this will increase by a factor of 5 – 10 the suppression for this kind of background. The full energy beam ions were not detected in the focal plane of the separator in all our experiments, and on this basis we estimate the suppression factor to be not worse than 10^{19} .

The described conditions allow us, with the use of the Si detector array, to establish the time and position correlations between the signals of recoil nuclei and their α decay for short-lived, $T_{1/2} = (5 \mu\text{s} - 1 \text{s})$ ER's. The α – α correlations occurring as a result of α –decay chains can be observed for the time intervals ranging from $1.5 \mu\text{s}$ to (10–100) s. The attainable upper limit depends on the α –energy and count rate. We use such correlations each time when a new nucleus is identified or excitation functions are measured for the known nuclei produced with a cross-section of ≤ 10 nb. Long lived nuclei with higher production cross-sections are recognized unambiguously due to their known α –lines.

5.2 Suppression of transfer reactions products

Complete fusion reactions are accompanied by a great number of multinucleon transfer reactions oftenly having larger cross sections than the production cross sections of ER's. The main problem is that the decay of the nuclides produced in transfer reactions interferes in the detection

Table 3. The suppression factors for the multinucleon transfer reactions products.

Reaction	Transfer reaction products	Beam energy (MeV)	w_t (mg/cm ²)	Suppression factors	References
$^{40}\text{Ar} + ^{238}\text{U}$	^{242}Cm	225	0.5 mg/cm ²	2×10^4	[28]
	^{227}Th			8×10^4	[29]
$^{40}\text{Ar} + ^{208}\text{Pb}$	^{211}Bi	196	0.6 mg/cm ²	7×10^3	[30]
$^{22}\text{Ne} + ^{248}\text{Cm}$	^{254}Fm	120	0.33 mg/cm ²	$\geq 4 \times 10^3$	[31]

of the radioactive decay of the fusion reaction products.

We investigated the suppression of the multinucleon transfer for the reactions $^{40}\text{Ar} + ^{238}\text{U}$ [27], $^{40}\text{Ar} + ^{208}\text{Pb}$ and $^{22}\text{Ne} + ^{248}\text{Cm}$ (see Table 3). The transfer reaction products obtained in the separator focal plane are listed in second column of Table 3. The beam energy and target thickness are given in third and fourth columns, respectively. In the last two columns the deduced suppression factors are presented together with the references to the papers reporting the total production cross sections of the studied transfer reaction products.

6 Brief review of VASSILISSA experiments

By detecting ER's of the compound nuclei obtained for a number (more than 20) of target projectile combinations we studied systematically cross section regularities, fission barriers and survival probability of highly excited neutron deficient nuclei with $82 \leq Z \leq 105$ [4, 32, 33]. The high sensitivity and selectivity of the separator for the slow ER's produced in asymmetric fusion reactions allow us to obtain excitation functions over a cross-sections range encompassing seven orders of magnitude. In our experiments we obtained xn, pxn and α xn evaporation residues in the range of the projectile energy extending from the Coulomb barrier to the values corresponding to the compound nucleus excitation more than 100 MeV. The list of heavy-ion fusion reactions studied in this work is given in Tables 4 and 6.

In fig. 6 the cross sections are shown for the reactions giving evaporation residues equally displaced from the β –stability line. The steep

Table 4. List of heavy ion fusion reactions studied in our experiments (compound nuclei with $83 \leq Z \leq 94$). For the cross section values presented without errors the overall accuracy is estimated to be $\pm 50\%$.

Reaction	CN	3n	4n	5n	6n	7n	8n	9n	10n
		σ_{max}	σ_{max}	σ_{max}	σ_{max}	σ_{max}	σ_{max}	σ_{max}	σ_{max}
$^{40}\text{Ca}+^{151}\text{Eu}$	^{191}Bi	2.6 μb	0.9 μb						
$^{40}\text{Ca}+^{153}\text{Eu}$	^{193}Bi	23 μb	30 μb						
$^{40}\text{Ar}+^{159}\text{Tb}$	^{199}Bi		16 mb						
$^{31}\text{P}+^{169}\text{Tm}$	^{200}Po	1.04 mb	4.51 mb	2.63 mb	4.25 mb	0.68 mb	320 μb	40 μb	9.5 μb
$^{27}\text{Al}+^{175}\text{Lu}$	^{202}Po	2.2 mb	17 mb	30 mb	8.4 mb	10 μb^{***}	5 μb^{***}		
$^{40}\text{Ca}+^{159}\text{Tb}$	^{199}At	3.6 μb				1.6 mb	0.22 mb	2.5 μb^{***}	0.4 μb^{***}
$^{40}\text{Ar}+^{165}\text{Ho}$	^{205}At			11.5 mb	2 mb	400 μb	35 μb	3.5 μb	
$^{24}\text{Mg}+^{181}\text{Ta}$	^{205}At			30 mb	4.5 mb	850 μb	54 μb		
$^{26}\text{Mg}+^{181}\text{Ta}$	^{207}At		14 mb	40 mb	20 mb	8 mb			
$^{22}\text{Ne}+^{194}\text{Pt}^{***}$	^{216}Ra		11 mb		3 mb		90 μb		
$^{22}\text{Ne}+^{196}\text{Pt}^{***}$	^{218}Ra		≥ 4.3 mb	20 mb	15 mb		1.5 mb		40 μb
$^{27}\text{Ne}+^{198}\text{Pt}^{***}$	^{220}Ra			25 mb	30 mb	18 mb	10 mb		1.0 mb
$^{20}\text{Ne}+^{197}\text{Au}$	^{217}Ac	145 μb			240 μb^*		2.6 μb^*		
$^{22}\text{Ne}+^{197}\text{Au}$	^{219}Ac		3 mb	6.5 mb	2 mb				
$^{24}\text{Mg}+^{197}\text{Au}$	^{221}Pa	200 nb	910 nb	600 nb	130 nb				
$^{26}\text{Mg}+^{197}\text{Au}$	^{222}Pa			2800 nb	1180 nb				
$^{22}\text{Ne}+^{205}\text{Tl}$	^{227}Pa	42 μb	96 μb	57 μb	31 μb				
$^{27}\text{Al}+^{197}\text{Au}$	^{224}U			4.7 ± 1.9 nb	1.6 ± 1.1 nb				
$^{20}\text{Ne}+^{208}\text{Pb}$	^{228}U		800 ± 400 nb	500 ± 300 nb					
$^{22}\text{Ne}+^{208}\text{Pb}$	^{230}U		6 ± 2 μb	2.5 ± 1 μb					
$^{22}\text{Ne}+^{209}\text{Bi}$	^{231}Np		300 ± 120 nb	70 ± 40 nb					
$^{24}\text{Mg}+^{208}\text{Pb}$	^{232}Pu		4 ± 2 nb						
$^{26}\text{Mg}+^{207}\text{Pb}$	^{233}Pu		30 ± 15 nb						
$^{26}\text{Mg}+^{208}\text{Pb}$	^{234}Pu		100 ± 50 nb	17 ± 8 nb					

* - the cross section values are presented as a sum of 4-5n, 6-7n and 8-9n channels, respectively.

** - a preliminary result

*** - the cross section value was measured at the fixed beam energy, which could be not at the maximum of the excitation function

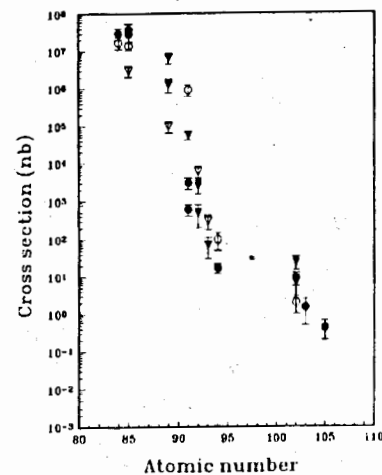


Fig. 6. Maximum cross section values from our experiments. 4n channel: \circ - Ne induced reactions, ∇ - Mg, Al induced reactions; 5n channel; \bullet - Ne induced reactions, \blacktriangledown - Mg, Al induced reactions.

decrease of the cross sections is observed in transition from thorium to uranium compound nuclei. A similar behavior was obtained also for pxn and α xn reactions. However, the step decrease obtained for α xn reactions is shifted to the transition from uranium to plutonium. This leads, in particular, to the fact that xn and α xn reaction channels are similar in the values of their cross sections for compound nuclei of Ac and Th on one hand and for Pu on the other. In contrast, in the case of the reactions leading to the compound nuclei of uranium the cross sections were detected in the microbarn region for 4n and 5n reaction channels whereas for α 2n, α 3n and α 4n reactions channels the obtained cross section values were close to millibarns. In fig. 7 the plot is shown of the cross-section values of different evaporation reaction channels as a function of the "loss" of the atomic charge obtained for the compound nucleus ^{224}U . The comparison is made for the reaction $^{27}\text{Al}+^{197}\text{Au}$, studied in our experiments, and for the more symmetrical one $^{40}\text{Ar}+^{184}\text{W}$ [34].

The discussion of the obtained step decrease of the evaporation reaction cross-sections was given in [4].

The obtained xn, pxn and α xn reaction cross sections were used for extraction the information about the fission barriers of neutron deficient $Z \geq 82$ nuclei [35, 36] and dependence of the $N = 126$ shell correction on the compound nucleus excitation energy [25, 37].

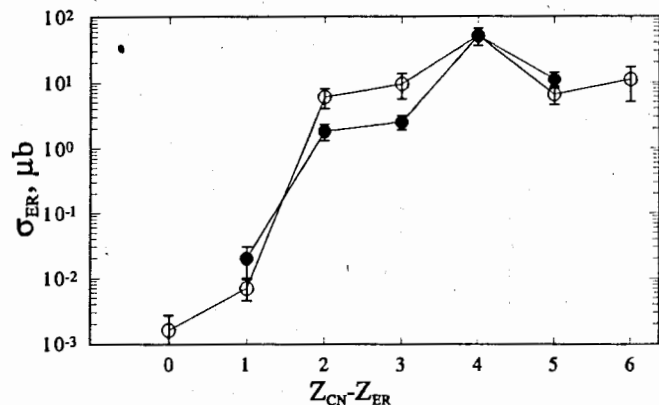


Fig. 7. Evaporation residue cross sections as a function of "charge loss" $Z_{CN} - Z_{ER}$; o $-^{27}\text{Al} + ^{197}\text{Au} \rightarrow ^{224}\text{U}^*$; • $-^{40}\text{Ar} + ^{184}\text{W} \rightarrow ^{224}\text{U}^*$.

New isotopes $^{218,219,223-226}\text{U}$, $^{225-227}\text{Np}$ and $^{228-230}\text{Pu}$ were produced and identified, and their α -decay energy and half life times were measured [38, 39]. For a few isotopes new data on α -decay energies or α -line intensities have been obtained. In Table 5 the list of the new isotopes, synthesized at the separator VASSILISSA, is given. More detailed data and comparison with the data of other authors can be found elsewhere (see, for example [38, 39] and refs. therein).

The method of recoil- α and α - α time and position correlation analysis was applied for the new isotope identification. The main experimental problem in these experiments was to identify ER's produced with the nanobarn cross-sections among the other nuclei (multinucleon transfer reactions products and ER's formed as a result of pxn and α xn reactions) produced with the cross-sections larger by more than 3 orders of magnitude. As an example in fig. 8 the α -spectrum is shown recorded in the experiment in which the new isotopes $^{228,229}\text{Pu}$ produced in the reaction $^{26}\text{Mg} + ^{208}\text{Pb}$ were identified. One can see the α -lines from implanted nuclei resulted from different multinucleon transfer reactions, namely $^{211m,211}\text{Po}$, $^{212m,212}\text{At}$ and from the reactions of α xn and 2α xn-type - $^{225,226}\text{U}$, $^{221-224}\text{Th}$ and their daughter nuclides.

The experimental conditions encountered at the synthesis of transfermium elements are the most difficult. This work sets the highest requirements for the experimental apparatus and accelerator. Nanobarn and subnanobarn values of the production cross sections of the nuclei lead

Table 5. The characteristics of new neutron deficient isotopes synthesized at the kinematic separator VASSILISSA.

Nuclide	E_α keV	I_α %	$T_{1/2}$ ms
^{218}U	8625 ± 25	100	$1.5^{+7.3}_{-0.7}$
^{219}U	9680 ± 40	100	0.042^{+34}_{-13}
^{223}U	8780 ± 40	100	$0.018^{+0.010}_{-0.005}$
^{224}U	8470 ± 15	100	$0.7^{+0.5}_{-0.2}$
^{225}U	7870 ± 20	100	30^{+20}_{-10}
^{226}U	7570 ± 20	85 ± 5	200 ± 50
	7420 ± 20	15 ± 5	
^{225}Np	8630 ± 20	100	
^{226}Np	8060 ± 20	50 ± 15	
	8000 ± 20	50 ± 15	
^{227}Np	7680 ± 20	100	
		EC < 25%	
^{228}Pu	7810 ± 20	100	
^{229}Pu	7460 ± 30	100	
^{230}Pu	7050 ± 20	100	

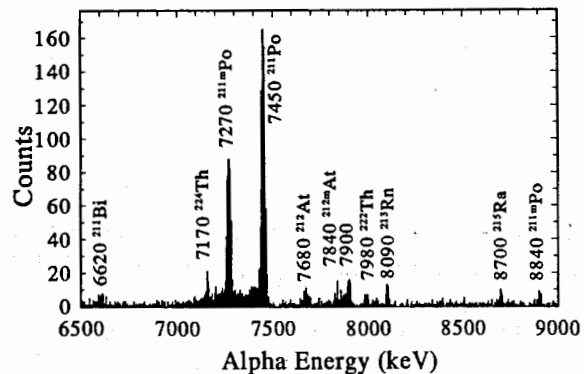


Fig. 8. α -spectrum from $^{26}\text{Mg}+^{208}\text{Pb}$ reaction at $E_{lab}=145$ MeV.

to the requirement of a high beam intensity and long (more than one week) irradiation time. During this long term experiments the highest possible background suppression factors and transport efficiency of the experimental set-up should be maintained.

The list of heavy-ion fusion reactions leading to the transfermium region and studied in our experiments is given in Table 6. The average beam intensity of ^{22}Ne , ^{26}Mg , ^{27}Al and ^{31}P ions varied between 0.5 and 1.0 μA . The silicon detector array installed in the focal plane of the separator allowed for the reliable identification of the $^{252-254}102$ isotopes having the production reaction cross-sections of > 1 nb. The cross section limit was reduced to 0.1 nb due to the position sensitivity of the detectors allowing the observation of mother-daughter correlations for $^{257,258}105$. Spontaneous fission (SF) branches associated with $^{252}102$ and $^{258}105$ were also observed. The α -decay branching ratio of ^{249}Fm $b_{\alpha} = (32.8 \pm 8.5)\%$ was obtained from the ratio of the number of its α -decays to that for the parent $^{253}102$. Fig. 9 presents some examples of the measured α -spectra.

The analysis of the measured cross-sections with the use of the ^{22}Ne , ^{26}Mg , ^{27}Al and ^{31}P projectiles did not reveal any evidence for a hindrance to fusion at the ion bombarding energy close to Coulomb barrier. More detailed consideration of the obtained results are presented in the [7, 5, 33].

Table 6. List of heavy ion fusion reactions studied in our experiments and leading to the compound nuclei with $Z \geq 102$.

Reaction	Channel	E_{cx} (MeV)	σ_{mar} (nb)
$^{22}\text{Ne}+^{236}\text{U}$	4n	45	7 ± 4
	5n	50	25 ± 7
	6n	57	15 ± 5
$^{26}\text{Mg}+^{232}\text{Th}$	4n	45	6 ± 2
	5n	50	9 ± 5
	6n	60	8 ± 3
$^{22}\text{Ne}+^{238}\text{U}$	6n	53	$15 \pm 7^{***}$
	8n	70	1.2 ± 0.8
$^{27}\text{Al}+^{232}\text{Th}$	5n	53	1.7 ± 0.5
	6n	60	1.3 ± 0.5
$^{27}\text{Al}+^{236}\text{U}$	5n	57	0.45 ± 0.2
	6n	65	$0.075^{+0.05}_{-0.06}$
$^{31}\text{P}+^{232}\text{Th}^{**}$	5n	56	0.12 ± 0.1

** - a preliminary result

*** - the cross section value was measured at the fixed beam energy, which could be not at the maximum of the excitation function

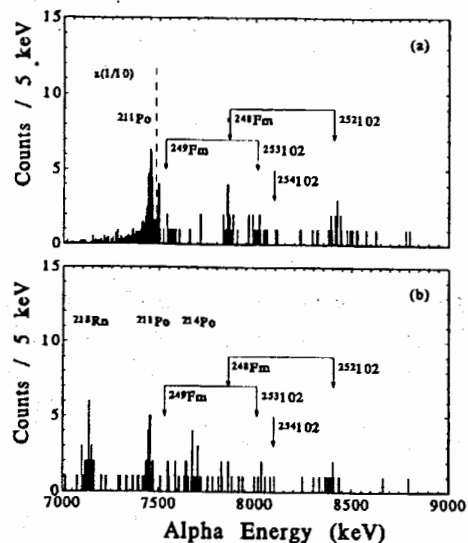


Fig. 9. α -spectra from $^{22}\text{Ne} + ^{236}\text{U}$ reaction at $E_{\text{lab}}=124$ MeV - (a) and from $^{26}\text{Mg} + ^{232}\text{Th}$ reaction at $E_{\text{lab}}=141$ MeV - (b) recorded between beam pulses.

7 Conclusion

The separator provides the high rejection factor ($\geq 10^{19}$) for the full energy beam ions. The main source of the background for the focal plane detector system originates from low energy (1 - 20 MeV) scattered beam ions. The overall background suppression factors ranges from 10^{13} - 10^{11} being dependent on the projectile to target mass ratio and also on the tuning of the cyclotron beam.

A running program planned for the implementation assumes the addition of a dipole magnet providing, after the separator, the 8° deflection for ER's. This will give probably an additional factor of 10 in the background suppression, and enable us to see the longer recoil-alpha correlation times and increase the life time of the Si detectors. The separator has a rotating wheel target synchronized with the cyclotron beam modulation. This target is capable of sustaining the beam currents of up to $3 \mu\text{A}$. Such currents of the bombarding ions in the Ne-Ar range allowing us to achieve the sensitivity of 100 pb in an one week experiment are provided

for by the U-400 cyclotron.

Acknowledgments

We thank A.N. Shamanin and V.A. Zakharov for their maintenance of VASSILISSA and the U-400 crew for providing the beams of high intensity.

References

- [1] A.V. Yeremin *et al.*, *Nucl. Instr. and Meth.* A274 (1989) p. 528.
- [2] A.V. Yeremin *et al.*, Preprint JINR E15-90-347, Dubna 1990.
- [3] G. Mützenber, Preprint GSI-92-76, 1992, to be published in: Handbook of Nuclear Decay Methods, CRC Press, eds.: W. Greiner and D.N. Poenaru.
- [4] A.N. Andreyev *et al.*, *Proc. Int. Symp. "Towards a Unified Picture of Nuclear Dynamics, Nikko, Japan, 1991"*, (New York: AIP) p. 499. Preprint JINR, E15-91-411, Dubna 1991.
- [5] A.N. Andreyev *et al.*, *Z. Phys.* A345 (1993) p. 389.
- [6] A.N. Andreyev *et al.*, *Z. Phys.* A344 (1992) p. 225.
- [7] A.N. Andreyev *et al.*, *Inst. Phys. Conf. Ser. No 132: Section 4*, p. 423. *Proc. 6th Int. Conf. on Nuclei Far from Stability & 9th Int. Conf. on Atomic Masses and Fundamental Constants*, Bernkastel-Kues, 1992.
- [8] R.N. Sagaidak, JINR Communication P7-89-551, Dubna 1989.
- [9] A.G. Popeko. *Nucl. Instr. and Meth.* (to be published).
- [10] N.K. Skobelev, V.Z. Maidikov, G.S. Popeko, Yu.V. Hoffman, O.F. Nemetz and Yu.Ts. Oganessian, *Yad. Fiz.* 29 (1979) p. 615.
- [11] K. Shima, S. Nagai and T. Ishihara, *Nucl. Instr. and Meth.* A244 (1986) p. 330.
- [12] A.B. Wittkower and H.D. Betz, *Atomic Data* 5 (1973) p. 113.
- [13] K. Shima, T. Mikumo and H. Tawara, *Atomic Data and Nuclear Data Tables* 34 (1986) p. 357.
- [14] K. Shima, N. Kuno, M. Yamanouchi and H. Tawara, *Atomic Data and Nuclear Data Tables* 51 (1992) p. 173.
- [15] V.S. Nikolaev and I.S. Dmitriev, *Phys. Lett.* A28 (1968) p. 277.
- [16] K. Shima, T. Ishihara and T. Mikumo, *Nucl. Instr. and Meth.* 200 (1982) p. 605.
- [17] A.G. Popeko, R.N. Sagaidak, A.V. Yeremin, *Proc. of the Int. School-Seminar on Heavy Ion Physics*, JINR E7-93-274, Dubna, 1993, V II.

- [18] R.N. Sagaidak and A.V. Yeremin, Preprint JINR E15-93-356, Dubna 1993, submitted to *Nucl. Instr. and Meth. B*.
- [19] A.V. Yeremin *et al.*, Inst. Phys. Conf. Ser. No 132: Section 8, p. 935. *Proc. 6th Int. Conf. on Nuclei Far from Stability & 9th Int. Conf. on Atomic Masses and Fundamental Constants*, Bernkastel-Kues, 1992.
- [20] A.N. Andreyev *et al.*, *Z. Phys.* A345 (1993) p. 247.
- [21] A.N. Andreyev *et al.*, *Z. Phys.* A338 (1991) p. 363.
- [22] A.N. Andreyev *et al.*, *Proc. Int. Conf. on Programming and Mathematical Methods for Solving Physical Problems*, JINR, Dubna, Russia, 14-19 June 1993.
- [23] PC NFS, Sun Microsystems, Inc., Reference Manual
- [24] R. Brun *et al.*, PAW - Physics Analysis Workstation. CERN Program Library Q121, CERN, 1992
- [25] A.N. Andreyev *et al.*, JINR Rapid Communications, 4[5]-91, p. 12, Dubna 1991.
- [26] A.N. Andreyev *et al.*, *Yad. Fiz.* 50 (1989) p. 619.
- [27] A.N. Andreyev *et al.*, JINR Rapid Communications No.3[29]-88, p. 33, Dubna 1988.
- [28] Yu.Ts. Oganessian *et al.*, Preprint JINR, D7-87-392, Dubna 1987.
- [29] U.W. Scherer *et al.*, Preprint GSI-89-85, Darmstadt 1989.
- [30] J.M. Nitschke *et al.*, *Nucl. Phys.* A313 (1979) p. 236.
- [31] D. Lee *et al.*, *Phys. Rev.* C25 (1982) p. 286.
- [32] A.N. Andreyev *et al.*, *Proc. of the Int. Conf. on Exotic Nuclei*, p. 191, Foros, Crimea, 1991, World Scientific Publ. Co. (Singapore).
- [33] A.V. Yeremin *et al.*, *Proc. of the Int. School-Seminar on Heavy Ion Physics*, JINR E7-93-274, Dubna, 1993, p. 109.
- [34] F.P. Heßberger, V. Ninov and D. Ackermann, *Z. Phys.* A343 (1992) p. 301.
- [35] G.M. Ter-Akopian *et al.*, *Nucl. Phys.* A553 (1993) p. 735c.
- [36] A.N. Andreyev *et al.*, *Yad. Fiz.* 56 (1993) p. 9.
- [37] A.N. Andreyev *et al.*, *Nucl. Phys.* A (1993) in press
- [38] A.N. Andreyev *et al.*, *Proc. of the Int. School-Seminar on Heavy Ion Physics*, JINR E7-93-274, Dubna, 1993, p. 493.
- [39] A.N. Andreyev *et al.*, Inst. Phys. Conf. Ser. No 132: Section 5, p. 759. *Proc. 6th Int. Conf. on Nuclei Far from Stability & 9th Int. Conf. on Atomic Masses and Fundamental Constants*, Bernkastel-Kues, 1992.

Received by Publishing Department
on March 3, 1994.